8

PIII for Aluminium Surface Modification

Régulo López-Callejas et al.*
Instituto Nacional de Investigaciones Nucleares, Plasma Physics Laboratory
A.P. 18-1027, 11801, México D. F.
México

1. Introduction

Aluminium is the third more abundant element in the Earth crust. The metal exhibits useful properties such as low density, high strength, good formability and a high resistance to corrosion. Aluminium can gain significant mechanical strength by means of alloying, whereby it is the most used metal after steel. In this sense, aluminium properties depend on its purity and its crystalline structure is face centred cubic [Wang et al, 1999].

Aluminium is, among other characteristics, malleable, easily machined and very ductile. Its high sensitivity to oxidation endows it with a waterproof passivation layer, typically 5-20μm thick according to the prevailing humidity, considerably adherent, which contributes to corrosion tolerance and general durability. The passivation layer consists of the amphoteric aluminium oxide Al_2O_3, often known as *alumina* or *aloxite* in mining and materials science. As corrosion is a major source of failure in Materials Engineering, aluminium is an obvious choice to face aggressive environments, including the atmospheric one.

Aluminium as a pure element has a low mechanical resistance which prevents its application under deformation and fracture conditions. Thus, low density combined with good resistance make aluminium alloys very attractive in design considerations. The properties of these alloys depend on a complex interaction among chemical composition, microstructural failures in solidification, thermal treatments, etc. although an increase in the alloy content tends, in general, to diminish the tolerance to corrosion. That is why quenching processes have been developed to improve the response to corrosion of highly alloyed materials. It is essential to select the precise alloy to match the resistance, ductibility, formability, solubility, corrosion tolerance, etc., required by an application.

Modifying aluminium composition by the adding nitrogen in an ion implantation process provides the treated samples with surface hardness and improved tribological properties by heating them in a nitrogen rich atmosphere. In this way, at low doses, aluminium nitride (AlN) becomes structured in the shape of clusters, the nitride content clearly increasing with the dose. Ion implantation is applied to pieces subjected to major friction and load forces such as rolling tracks, cylinder sleeves, etc., which require some core plasticity enabling

* Raúl Valencia-Alvarado[1], Arturo Eduardo Muñoz-Castro[1], Rosendo Peña-Eguiluz[1], Antonio Mercado-Cabrera[1], Samuel R. Barocio[1], Benjamín Gonzalo Rodríguez-Méndez[1] and Anibal de la Piedad-Beneitez[2]
[1]*Instituto Nacional de Investigaciones Nucleares, Plasma Physics Laboratory A.P. 18-1027, 11801, México*
[2]*Instituto Tecnológico de Toluca A.P. 890, Toluca, México*

them to absorb vibrations and impacts, but maintaining their high surface hardness against wearing and deformation [Manova et al, 2001].

AlN was first synthesised in 1877. It is mostly formed by covalent bonds and exhibits a hexagonal crystalline structure which is isomorphic to the wurzite form of zinc sulphide. AlN is stable at very high temperatures in inert atmospheres. Its surface oxidation in air takes place at 700°C, although 5-10 nm layers developed at room temperature have been detected [Selvaduray and Sheet 1993]. This layer protects the material above 1370°C. AlN is stable in hydrogen and carbon dioxide atmospheres even at 980°C. It dissolves slowly in mineral acids, which attack its grain borders, and in strong alkalis that react with the grain itself. AlN is gradually hydrolysed but it is resistant to several fused salts such as chlorides and cryolites.

The experimentation discussed in the present chapter concerns the alloy composition of aluminium 6061 containing Mg and Si as shown in Table 1. With a view to evaluating the content per element and assessing the crystalline phases identified by DRX in each aluminium 6061 sample, micographs (figure 1) and corresponding spectra (figure 2) were obtained by SEM. The diffractogramme of the control (reference) sample, seen in figure 3, presents aluminium peaks at the 2θ values: 38.47°, 44.74°, 65.13°, 78.23° and 82.43° (JCPDS 4-0787 standard) the last peak showing a greater intensity than that reported on Table 2. Aluminium oxide (Al_2O_3) can be detected at the 2θ angles 34.60°, 36.49°, 40.22° (JCPDS 12-0539 standard) and at 42.76° (JCPDS 24-0493 standard).

	%Si	%Fe	%Cu	%Mn	%Mg	%Zn	%Ti	%Cr	%other	%Al
6061	0.4-0.8	0.7	0.15-0.40	0.15	0.8-1.2	0.25	0.15	0.04-0.35	0.15	Balance

Table 1. Al 6061 composition

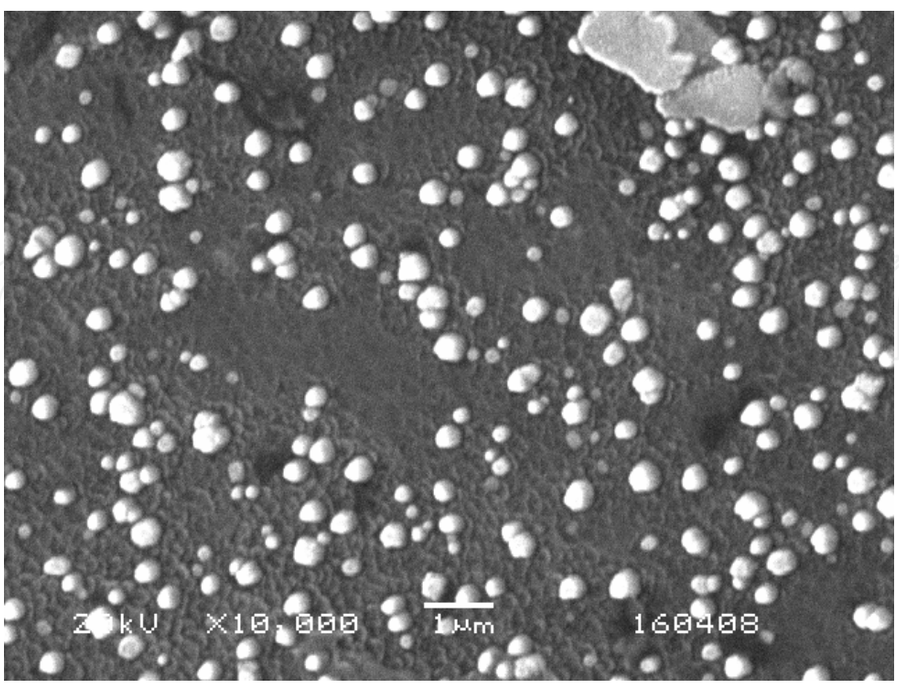

Fig. 1. Reference simple micrograph

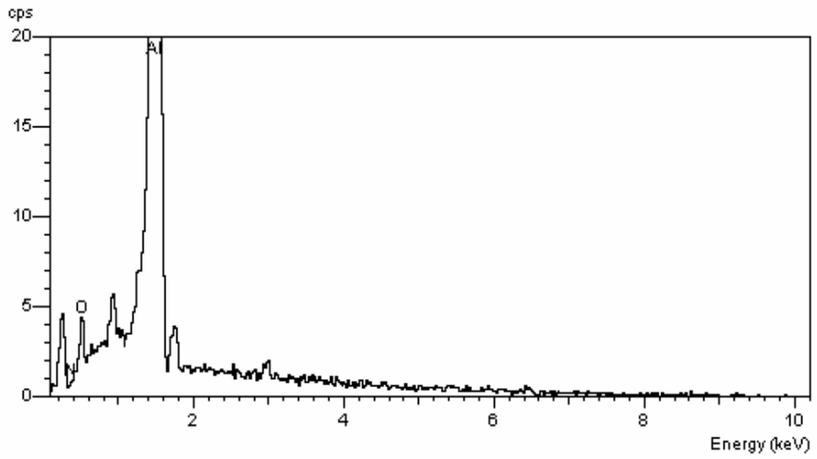

Fig. 2. Reference simple spectrum

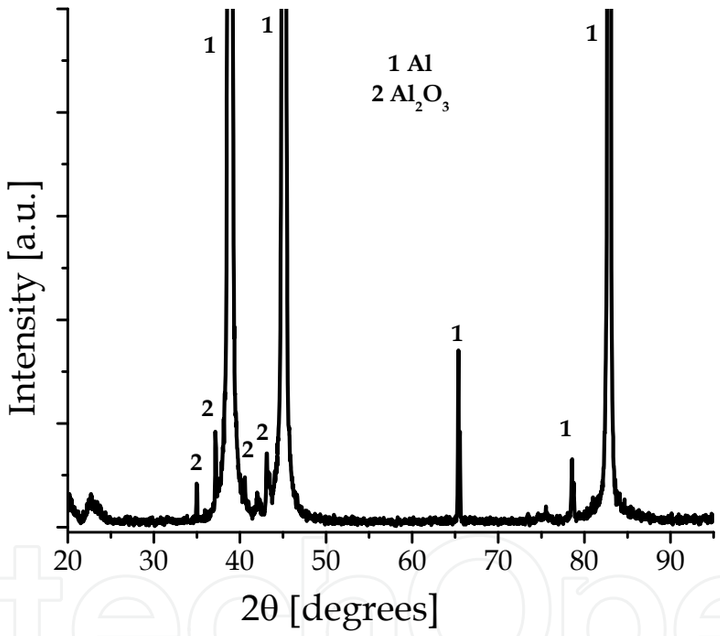

Fig. 3. Reference simple diffractogramme

Angle (2θ)	Relative intensity
38.47°	100
44.74°	47
65.13°	22
78.23°	24
82.43°	7

Table 2. Al peaks (JCPDS 4-0787 standard)

All in all, Aluminium and its alloys are attractive materials to the car, aviation, food and chemical industries as much as the pharmaceutical research. However, these materials lack surface hardness and other tribological qualities which limit their application nitriding is an effect time surface modification used to enhance corrosion tolerance in addition to wear resistance. In this chapter, a study of the formation of aluminium nitride (AIN) by means of the Plasma Implantation Ion Immersed (PIII) is presented.

2. Plasma immersion ion implantation process

Ion implantation based on linear accelerator technology has been long developed to modify material surfaces. The large implantation areas required by industrial applications and the extended processing times demanded by the treatment have made this implantation modality both expensive and complex, limiting its usefulness. By contrast, PIII technology [Conrad et al. 1987] overcomes many of the linear accelerator shortcomings providing a high ion density in a simple, fast, effective and economical way.

The PIII process has been amply described in several papers [Conrad et al. 1987], [Anders, 2000]. A brief description of it can follow. The sheath that normally surrounds an unbiased conductor (sample) submerged in plasma is characterised by an excess of electrons, no matter that the plasma is initially (t=0) in quasi-neutrality. When a voltage pulse, typically a few microseconds long, is applied to the "sample", the sheath is drastically altered and can even vanish momentarily. The comparatively small inertial mass of the electrons allows them to be expelled from the close vicinity of a cathode sheath, or negatively biased "sample", in a very short time. Consequentially, the ion array, or matrix, becomes exposed thanks to the ion's greater inertia. Later on, this charge distribution is enhanced as further electrons are repelled to the point in which the electric field of the biased "sample" is completely shielded. Thus, few centimetres away from the close vicinity of the "sample", the plasma remains unaltered, with the possible exception of the plasma waves created by the bias pulse.

The "sample" bias originates a short distance positive charge gradient and, with it, a potential gradient, namely, the electric field which impulses the ions towards the "sample". Once the ion matrix appears, a steady ion current flow onto the piece, to the extent of the availability of ions in the matrix. As the ions are implanted, the piece emits additional electrons according to its work function and, clearly, to the ion energy. The loss of these electrons extends the sheath by uncovering more ions. The bias pulse width and plasma density are usually adjusted in order, for as many sheath ions as possible, to be implanted into the piece, which is kept, therefore, immerse in the plasma. At the same time, the plasma represents a load to the high voltage pulsed energy supply which bias the work piece. By the end of the few microsecond pulse, the ion matrix is depleted and the system returns to very much the same initial conditions previous to t=0.

Conventional beam-line ion implantation has proven to modify significantly the surface properties of different materials. Nevertheless, PIII offers an alternative to conventional beam-line ion implantation. It has shown the advantages of relative simplicity, high ion fluence, the possibility of implanting complex three-dimensional objects, achieving an area treatment independent of the processing time and providing safe low temperature processing. By contrast, PIII is limited by the lack of charge to mass separation, having an implant energy distribution non homogeneous and the generation of X-rays from the production of secondary electrons.

3. Instrumentation for PIII process

This section contains a detailed description of the instrumentation used to carry out the PIII on the vacuum chamber with biased electrode, a specific high voltage modulator, and the diagnostic systems enabling to estimate the plasma parameters.

3.1 Vacuum chamber

To accomplish the PIII process, the device was designed and constructed as shown schematically in figure 4. The plasma is produced in a stainless steel cylindrical vacuum chamber 0.6 m high, 0.3 m in diameter and 5 mm thick in the wall; thus the vacuum chamber volume is 0.042 m^3. It has been provided with different ports for: a) pressure sensor, b) gas injection, c) electrode bias, d) target support, f) electrical probe diagnostics, g) spectroscopy diagnostics, along with other ports for future needs. The vacuum system consists of a turbo pump with a 500 l/s capacity.

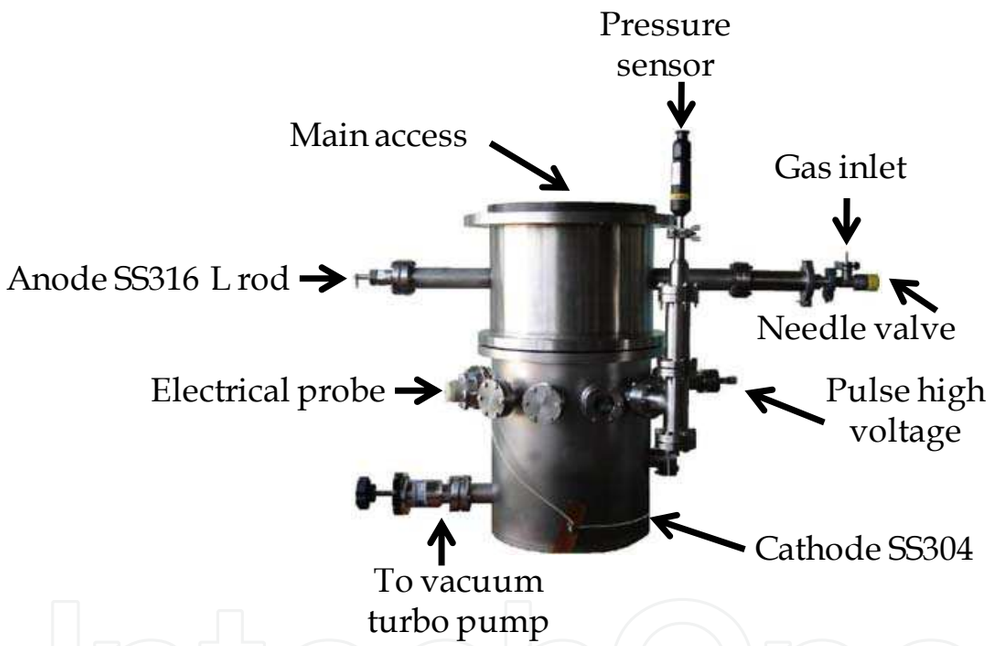

Fig. 4. General view of the vacuum chamber discharge and its main accessories

3.2 Plasma bias

The plasma is generated by a DC glow discharge between a stainless steel solid cylinder, acting as an anode, and the vacuum chamber as a cathode (figure 4). The DC power supply ranged within 0-1200 V/2A. The gas admission control to the vacuum chamber drives a gas dosing valve and the work gases being nitrogen and argon. The whole device is typically operated at a 1×10^{-6} Torr as base pressure and, during the PIII process, the work pressure falls into the 10^{-2} to 10^{-1} Torr interval.

3.3 Pulse generator chamber

The pulse CD supply (see figure 5) consists of a three phase full wave rectifying circuit (D1-D6) coupled to a Variac which enables the user to select the CD output voltage level. Later

on, the voltage is filtered so to supply the high voltage pulse transformer with a CD signal bearing the least possible ripple. The selected commutation device is an IGBT SKM200GB125D by SEMIKRON™ that is driven by an M57959L module. This is a high speed component endowed with a voltage logic level input and insulated by a high speed opto-coupler protected against the event of a short circuit. A commuted converter in a flyback configuration was chosen to build it, due to its relative simplicity and low cost.
The control stage has been implemented by a SG3527A pulse wave modulator (PWM) which imposes the width and repetition rate of the pulses applied to the M57959L module. According to the circuit configuration, the PWM work cycle can vary between 0 and 49% at a 55-2600 Hz rate. Such characteristics can be set up by the P1 and P2 potentiometers.

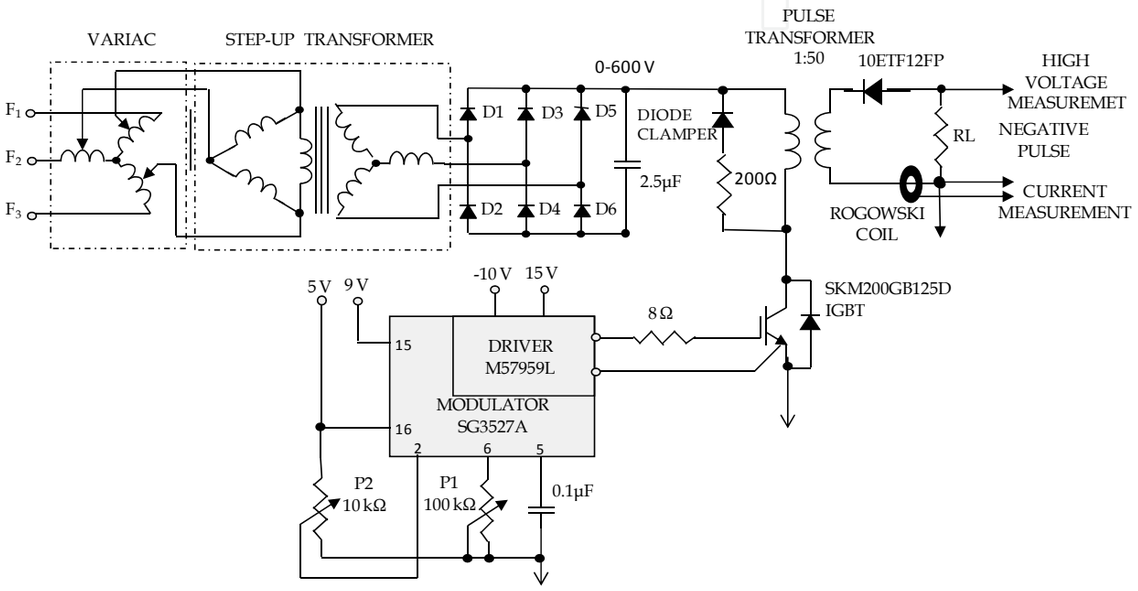

Fig. 5. High voltage pulse generator diagram

3.4 Electric probe diagnostics

In order to measure plasma parameters such as electron temperature (T_e) and plasma density (n) in a simple way, a double Langmuir probe is used. In order to increase the lifetime of the probe, a mechanical system (guard) was designed and constructed. This guard protects the electric probe within the chamber when the diagnostics is not being carried out. The probe is exposed to the plasma discharge for short intervals and only when the diagnostic system is activated. A probe was built out of an alumina rod with two perforations as the insulating element between two tungsten conductors and the metallic capsule that gives support to the probe (figure 6). The tungsten filaments are 0.195 mm in diameter and 4.3 mm long. The probe, inside the guard, is made of a stainless steel pipe, 0.95 cm in diameter and 25 cm long, intended to couple to the engine system that shifts the guard on and off.
This double probe was biased by means of a specifically designed and constructed triangular and sawtooth waveform generator operating in either modality thanks to the SW2 switch (see figure 7). An XR2206 function generator, and associated electronic components, was also used at the low voltage (±15V) stage so that a two scale frequency

output is obtained, due to the SW1 switch, between 0.2 and 20Hz and between 20 and 2000 Hz. The voltage is applied to the double probe in the order of ±150V by two STK4050V high voltage operational amplifiers connected in a differential way. Each amplifier was individually configured as an inverter with a gain factor of 47, given the relationships R17/R16 and R27/R26. Consequentially, the output peak value is ±75 V when 1.6Vp are applied at the amplifier input.

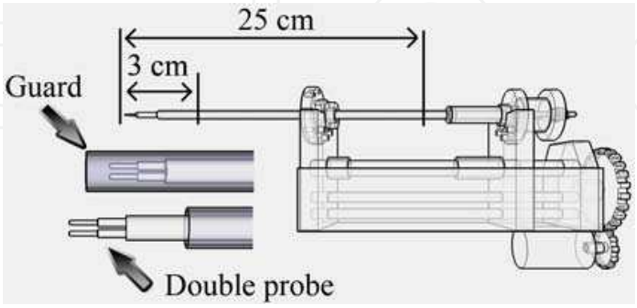

Fig. 6. Longitudinal positioning mechanism of the probe

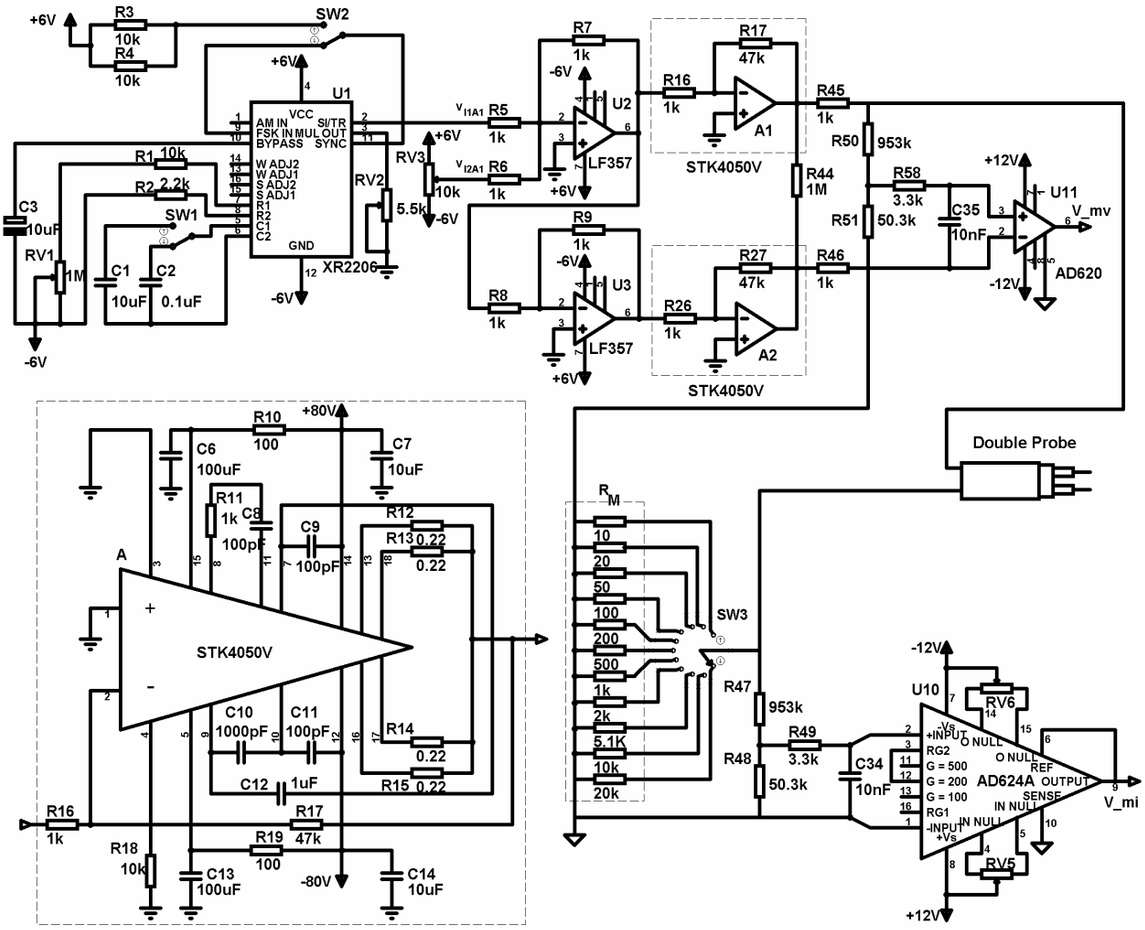

Fig. 7. General electronics circuit diagram

The data acquisition of the voltage and current signals from the signal conditioning stage was carried out with a DAQ PCI-6023E National Instruments board. The measurement of the current circulating through the plasma immerse probe was achieved by the use of an R_M, resistor. Thus, when the current varies between $\pm I_M$, a $\pm V_M$ voltage will be obtained in a directly proportional way. This voltage is located at the amplification stage input with a gain factor G_{AMP}=200. Then, assuming a maximal voltage limit at the board $V_{OA(MAX)}$, a sensor resistance R_M and an attenuation factor F_A, the expression of the maximal current interval $I_{M(MAX)}$ can be given by:

$$I_{M(MAX)} = \frac{V_{OA(MAX)}}{R_M F_A G_{AMP}} \tag{1}$$

The attenuation network (R47 and R48) of the current sensor where the low pass filter (R49 and C34) output signal is connected to the AD624 instrumentation amplifier. In this way, the I_M proportional V_M voltage signal is increased to a 200 gain. Once conditioned, the signal complies with the voltage specifications of the DAQ PCI-6023E acquisition board.

The probe displacement has been achieved by means of a longitudinal positioning mechanism allowing the guard, containing the double probe, to be introduced to the reactor as much as 25 cm while allowing exposing or retracting a 3 cm long tip of the probe with respect to the guard (figure 6).

A LabVIEW™ compatible program was specifically designed to operate the system. The software was applied to process, visualise and storage: the applied voltage, response current and probe positioning. The latter is set at the graphic interface (figure 8.a) which transmits the advance, stop and retreat signals, through an 8 bit terminal provided by the DAQ PCI-6023E board, to the power electronics associated to the mechanism. Then, a fraction of the collected current is selected in order to be plotted against the applied voltage and, from this characteristic curve, determining the main plasma parameters (figure 8b).

The saturation current and the electron temperature provide valuable information in determining the plasma parameters. Two values are calculated from the locus of the V-I plot, both from its positive and negative parts. The V-I double symmetrical cylindrical probe characteristic curve can be approached by the nonlinear function (Equation 1). The Levenberg-Marquardt fit method was implemented so to determine the coefficients of it [Herman and Gallimore, 2008]:

$$I(V) = I_{isat} \tanh\left(\frac{V}{2T_{eV}}\right) + A_1 V + A_2 \tag{2}$$

here, T_{eV} is the electron temperature [eV], I_{isat} is the saturation ion current [A] of each one of the probe ends, A_1 is an account of the expanded ion saturation current sheath depth, whereas A_2 refers to the reflection and displacement currents resulting from stray capacitances. The density calculation was performed on the basis of two types of data analysis: Bohm Approximation and Orbital Motion Limit (OML), given respectively by [Herman and Gallimore, 2008]:

$$n_i = \frac{I_{isat}}{0.61 A_S e}\sqrt{\frac{m_i}{kT_{eV}}} \tag{3}$$

$$n_{OML} = \sqrt{\frac{[-\Delta(I_i^2)/\Delta V_p]m_i}{0.2e^3 A_p^2}} \tag{4}$$

where A_S is the area of sheath [m²], e is the electron charge [C], m_i is the mass of ion [kg], k is Boltzmann´s constant [J/K], I_i is the ion current [A], V_p is the probe bias voltage [V], and A_P is the exposed probe electrode surface area [m²].

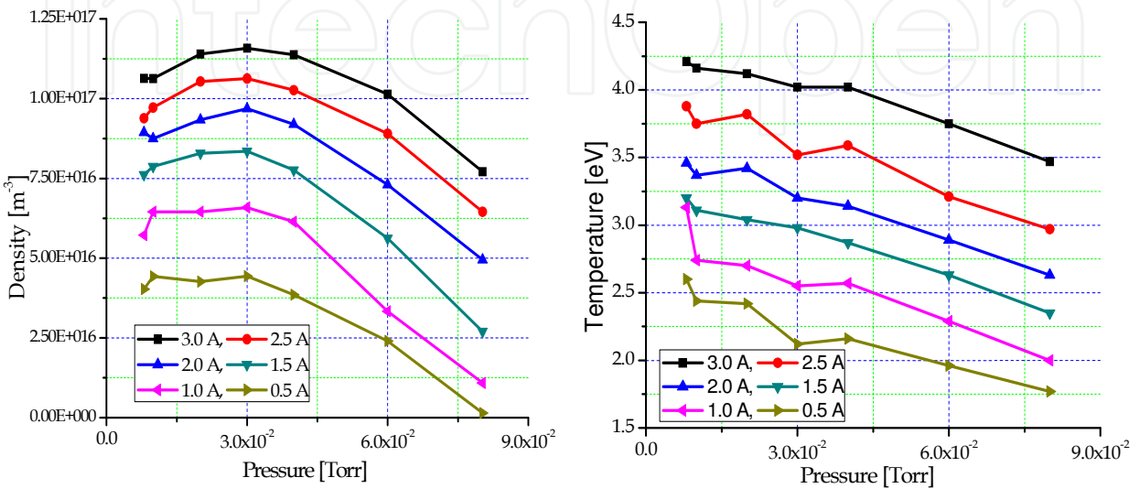

(a) Density (b) Temperature

Fig. 8. Nitrogen plasma parameters in DC

Instrumentation hardware and software have been calibrated on DC plasmas from argon, nitrogen and gas mixtures. Figure 8 displays some results obtained when the probe reached the centre of the reactor filled with nitrogen. The DC current supply went from 500mA to 3000mA, both cases being a function of the work pressure.

In a typical experiment under the previously specified plasma parameters, the following steps are conducted by means of the electric probe. First, the guard and electrical probe array are positioned inside the vacuum vessel, and, as a second step, the probe is moved outside the guard, putting it in contact with the plasma. When the electric probe stops, it is biased by one cycle of the sawtooth signal. With the electric probe system in position, it is possible to measure the electron density and temperature at different locations inside the vacuum chamber. The graphics shown in figure 8 correspond to the centre of the chamber.

3.5 The non collisional ion sheath model

Plasmas are ionised gases and, therefore, electrically conductive to some extent. In this way, plasmas are capable to shield regions of a scale estimated by the Debye length (λ_{De}) provided that the number of charged particles within the Debye sphere is far greater than one and that their motion obeys forces essentially electromagnetic. Other assumptions of the model are [Anders, 2000]:

- The ion flow is not collisional which apply to low gas pressures.
- Electrons are massless so that they respond instantly to the applied potentials given that the implantation time scale is much greater than the plasma cyclotron frequency ω_e.

- A bias $-V_0$ is applied to the piece at t=0, where V_0 >> T_e (with T_e clearly expressed in volts) whereby λ_{De} << s_0 the latter being the initial sheath depth.
- A quasi-static matrix is formed instantly demanding a current which satisfies Child's law and is provided by the uncovered ions nearby.
- The transit time through the matrix is null, i.e., the implantation current is identical to the amount of ion charge uncovered per second.
- All charged particles are singly ionised.

In this manner, the Child's law current density at a voltage V_0, through a sheath of thickness s, can be expressed as

$$j_c = \frac{4}{9}\frac{\varepsilon_0 (V_0)^{3/2}}{s^2}\sqrt{\frac{2e}{M}} \tag{5}$$

where ε_0 is the vacuum permittivity, e is the electron charge and M the ion mass. By equating j_c with the amount of charge per unit of time and per unit of area that crosses the sheath border, $en_0(ds/dt)$, one can find the expansion speed of this border:

$$\frac{ds}{dt} = \frac{2}{9}\frac{{s_0}^2 u_0}{s^2} \tag{6}$$

where $s_0 = \sqrt{(2\varepsilon_0 V_0)/en_0}$ is the ion matriz thickness and $u_0 = (2eV_0/M)$ is the characteristic ion speed. Equation (6) becomes, after integration,

$$s(t) = s_0\left(1 + \frac{2}{3}\omega_i t\right)^{1/3} \tag{7}$$

where $\omega_i = \sqrt{e^2 n_0/\varepsilon_0 M} = u_0/s_0$ is the ion frequency of the plasma.

Estimating the ion matrix thickness during a PIII process is crucial as its size must not approach the reactor dimensions (see section 3.1) in order to have enough plasma to collect and implant ions from. Figure 9 illustrates the dynamic evolution of the ion sheath in the case of nitrogen (M=28) when the bias potential $-V_0$ ranges from 1kV to 8 kV, provided that the plasma density is 9×10^{16} m^{-3} (cf. figure 8.a).

By integrating Eq. (5), the ion fluence F impinging on the aluminium piece can be calculated. In a planar geometry with a maximum sheath width $s(t)$ and a voltage V_0 during a pulse of length t_p, the fluence is:

$$F = n\left(s(t) + t_p\sqrt{\frac{kT_e}{M}}\right) \tag{8}$$

Typically, in a 50 μs pulse, a plasma density of 9×10^{16} m^{-3}, T_e =3eV and voltage of 5 kV, the fluence density can reach up to 1.7×10^{16} ions per m^2. With a 500 Hz repetition rate, it is possible to implant doses in the order of 10^{21} ions/m^2 in ~1 hour.

4. Results and discussion

The experimentation was carried out on a commercially pure aluminium rod (6061-T6) sectioned into cylindrical pieces, 10 mm in diameter and 5 mm thick. The samples were mirror

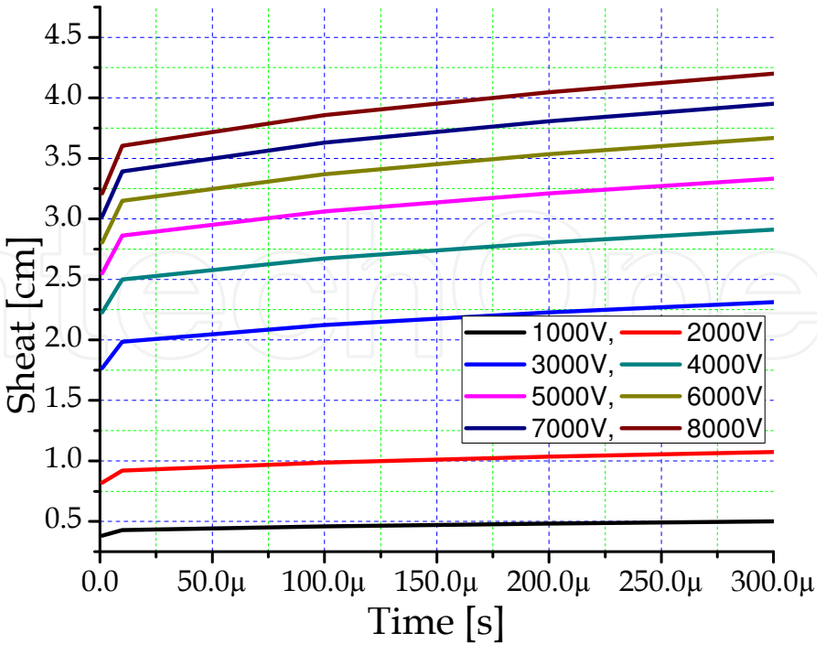

Fig. 9. Ion sheath evolution at a 9×10^{16} m^{-3} plasma density and biasing between -1 and -8 kV

polished and ultrasonically cleansed in acetone. A base pressure ~10^{-6} Torr was achieved with a turbo-molecular vacuum pump, and then the work pressure was established at 3×10^{-2} Torr (see figure 8.a) by admitting nitrogen of a 99.998% purity and its mixtures. Each sample receives a previous 30 min cleansing stay in Argon plasma to be finally implanted for 1-1.5 h periods. The PIII process was conducted with -2 to -5.5 kV bias squared pulses, with ion doses in the order of 1.7×10^{16} ions/cm^2 per pulse, while the electron plasma density is kept at about $9x10^{16}$ m^{-3}. The gas admission mixture was calibrated by using flow regulators. All the specimens were treated at 400°C. The samples were treated in four separate groups under previously optimised controlled conditions: the first one in 99.998%pure nitrogen (N), the second one in 70%Nitrogen and 30%Argon (70N-30A), the third one in 50%Nitrogen-50%Argon (50N-50Ar) and the last one in 30%Nitrogen-70%Argon (30N-70Ar) mixtures.

4.1 Aluminium treated at 2kV and 150 µs width pulse

The first treatment was applied during 1h periods at a 500 Hz repetition rate. The resulting micrographs are shown in figure 10 and the corresponding EDX spectra in figure 11. O, N and Al are always present in this specimen.

The micrograph in figure 10.d (N30-Ar70) presents a smoothed surface due to the intense bombardment with Ar, which is corroborated by the respective rugosity plot (figure 12). Likewise, the smoothing of the surface in micrograph 10.a follows from the N treatment. In the case of the N50-Ar50 mixture (figure 10.c) the grain size appears particularly inhomogeneous, with an average magnitude of 0.35 µm. Spiked grains of different sizes confirm the highest rugosity (R_a) values occurring in this lot of specimens. As the nitrogen bombardment intensity decreases, the hardness declines, except in the case of N50-Ar50 which displays the highest hardness (figure 13). This result could be explained from the

absence of aluminium oxide in the N70-Ar30 and N50-Ar50 treated samples with respect the pure nitrogen and N30-Ar70 cases. All the treated samples improve their hardness with respect to that of the untreated one, with the exception of the N30-Ar70 case which exhibits only the cubic crystalline phase, while the rest do both the cubic and hexagonal phases.

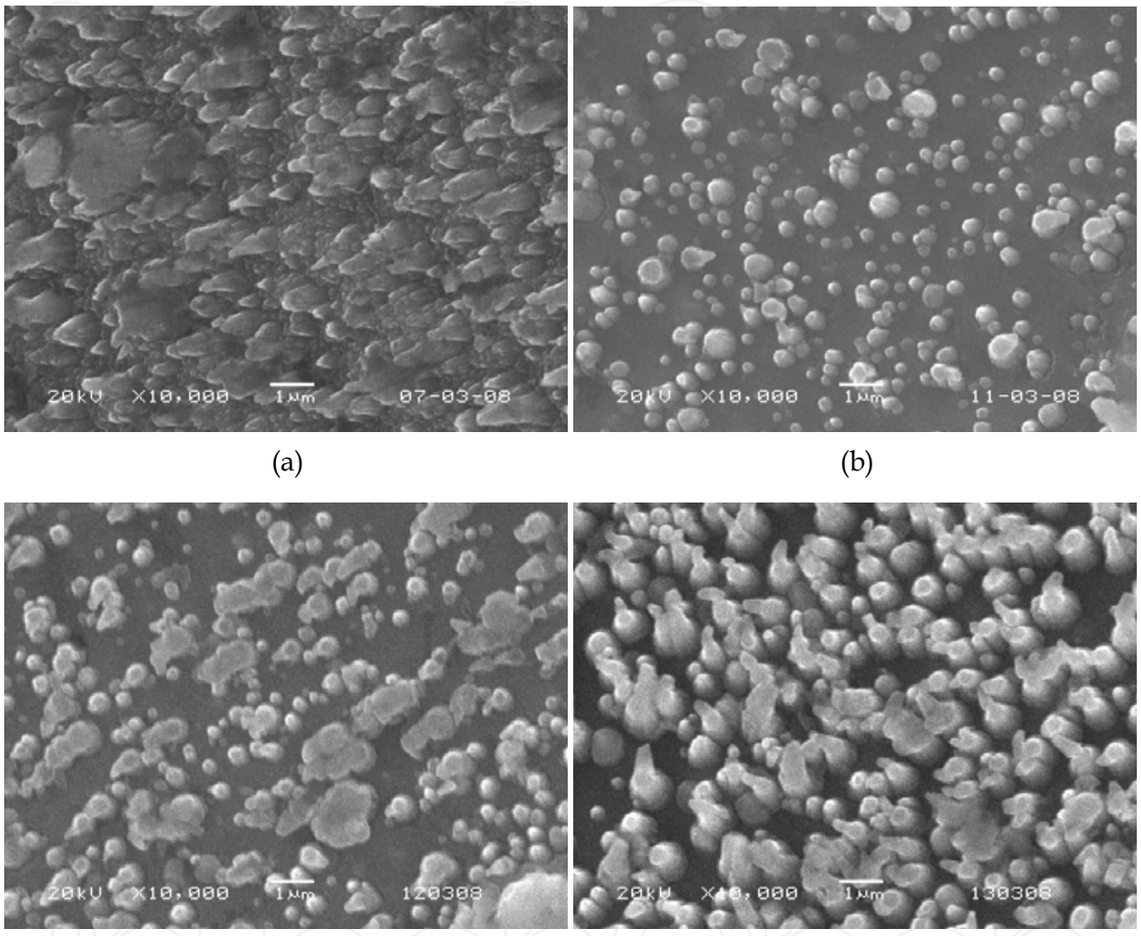

(a) (b)

(c) (d)

Fig. 10. Treatment micrographs: (a) Ar(N), (b) Ar/(N70-Ar30), (c) Ar/(N50-Ar50), (d) Ar/(N30-Ar70)

Diffractogramme 14.a, corresponding to N, shows the highest presence of AlN, both in cubic and hexagonal phases. Figure 14.c identifies the highest content of AlN in the cubic phase, as the presence of Ar seems to promote this phase and to inhibit the hexagonal one. This fact is due, perhaps, to the catalytic potential of argon, even though there is a competition between sputtering and implantation. In figure 14.b and 14.d, one observes only a small peak of the cubic phase of AlN. Thus, the high treatment temperature (400°C) may have changed the surface microhardness unfavorably, compared with the untreated case. The insignificant content of phases may be due to the relatively high sputtering produced by Ar in contrast with the nitrogen implantation.

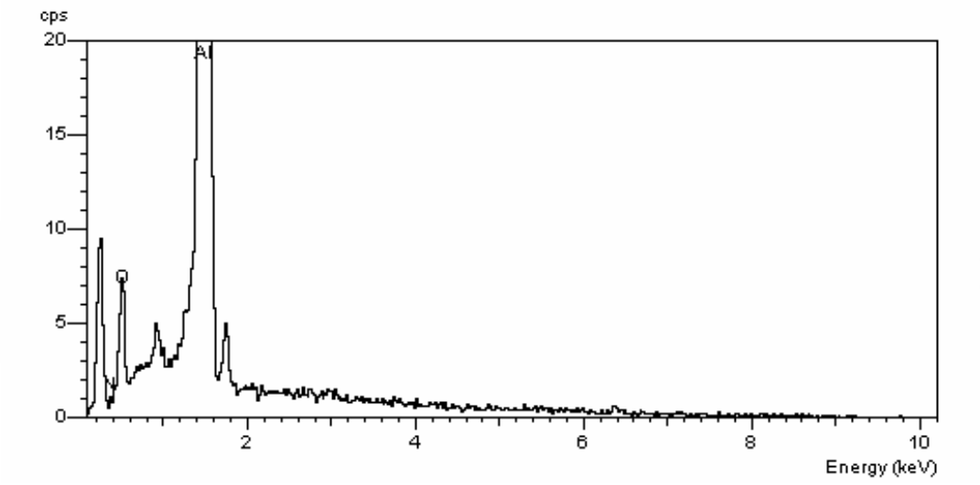
cps
20
15
10
5
0
Al
O
2
4
6
8
10
Energy (keV)

(a)

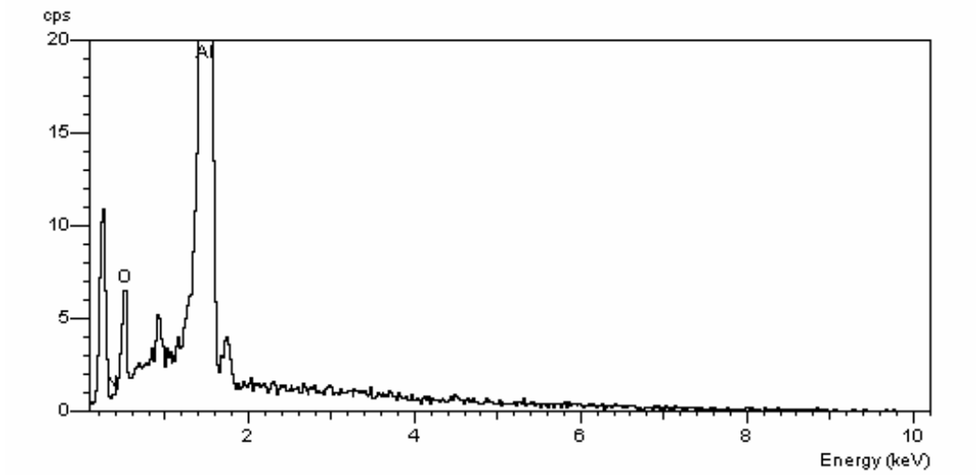
cps
20
15
10
5
0
Al
O
2
4
6
8
10
Energy (keV)

(b)

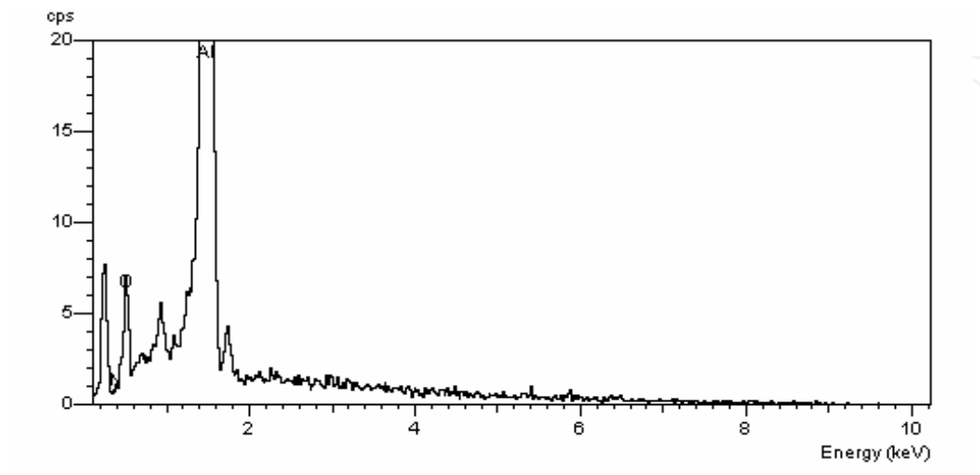
cps
20
15
10
5
0
Al
O
2
4
6
8
10
Energy (keV)

(c)

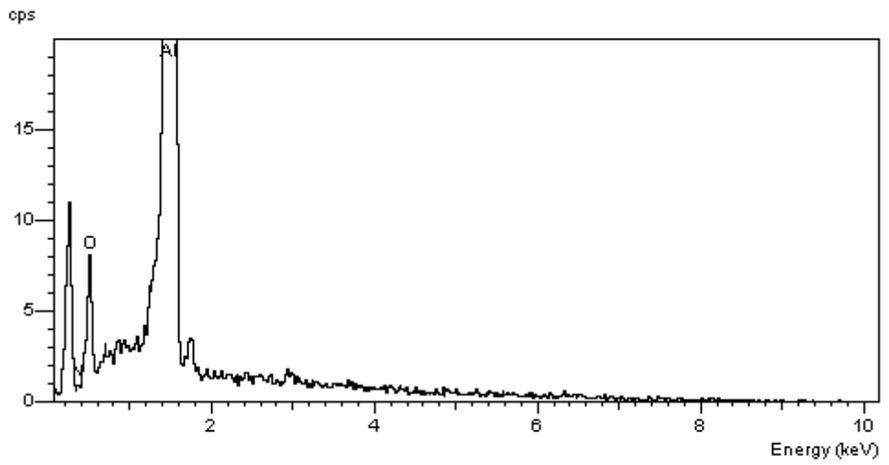

(d)

Fig. 11. Aluminium spectra: (a) Ar(N), (b) Ar/(N70-Ar30), (c) Ar/(N50-Ar50), (d) Ar/(N30-Ar70)

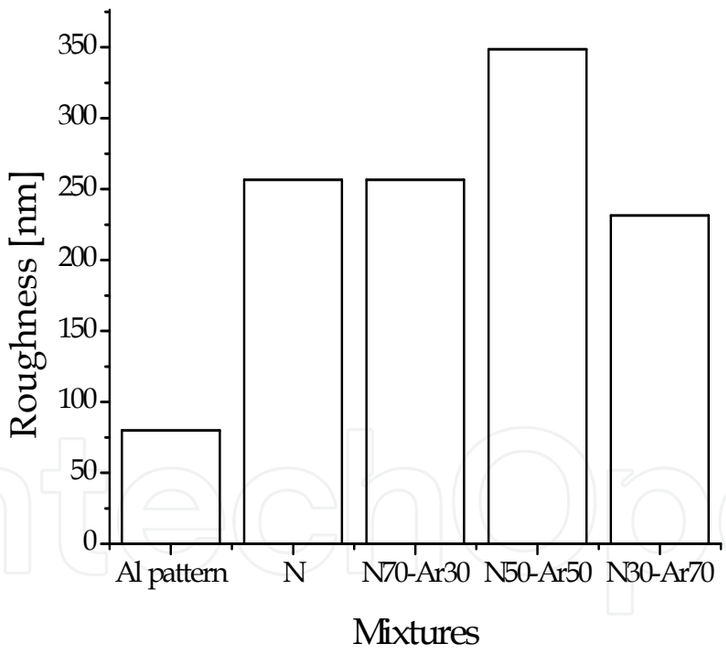

Fig. 12. Rugosity

4.2 Aluminium treated at 3.5kV and 75 µs width pulse

These tests were aimed at attracting the ions with greater energy by increasing the bias voltage while reducing the pulse width. The resulting micrographs are presented in figure 15. The maximal rugosity is identified in the sample treated with the Ar/(N30-Ar70) mixture (figure 15.c) given the respective rugosity tests (see figure 17). The changes in the morphology of the Ar/(N70-Ar30) and Ar/(N50-Ar50) treated samples, given that of the

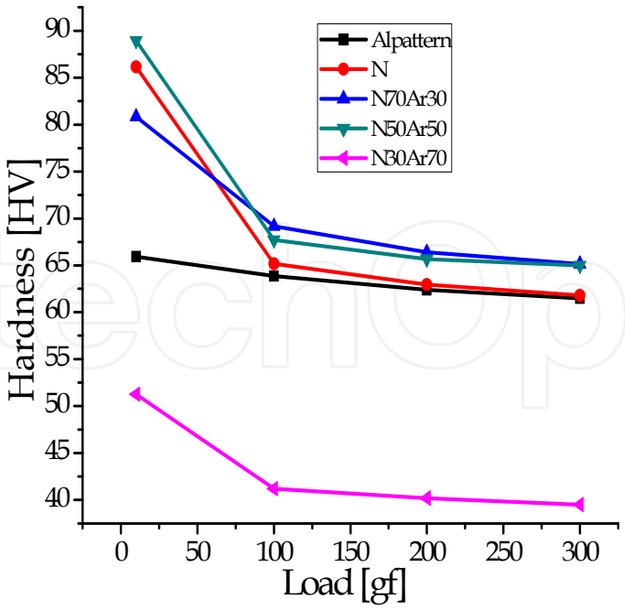

Fig. 13. Hardness

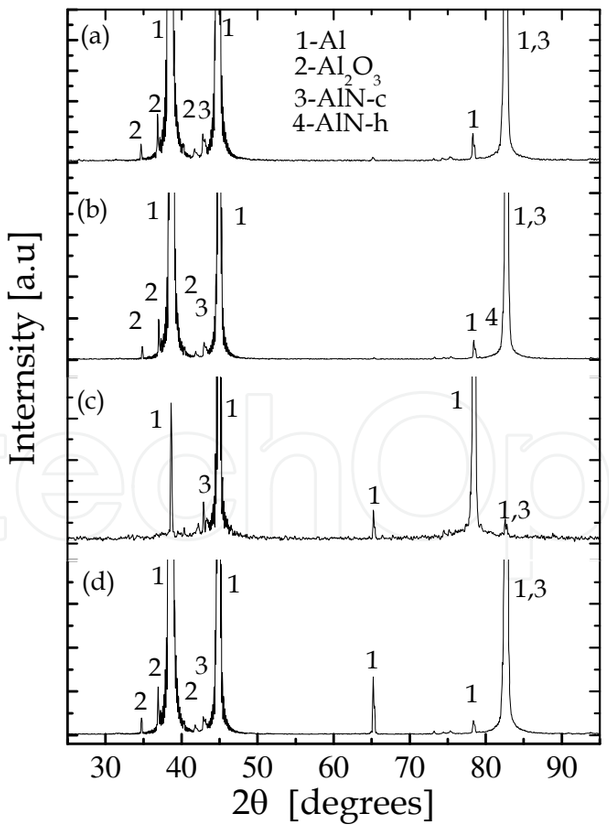

Fig. 14. Difractogrammes from: (a)Ar/(N), (b) Ar/(N70–Ar30), (c) Ar/(N50–Ar50) and (d) Ar/(N30–Ar70)

control one (figure 1) are evident. Figure 16 displays the EDS outcome suggesting the presence of N and an increase in O.

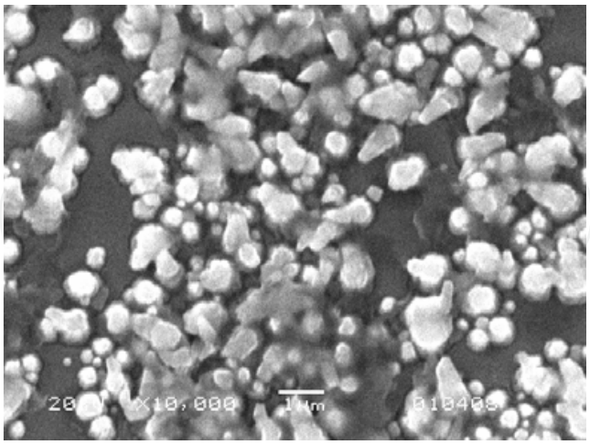

(a)

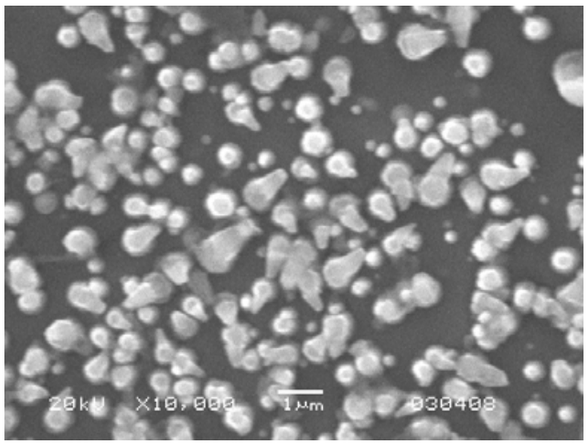

(b)

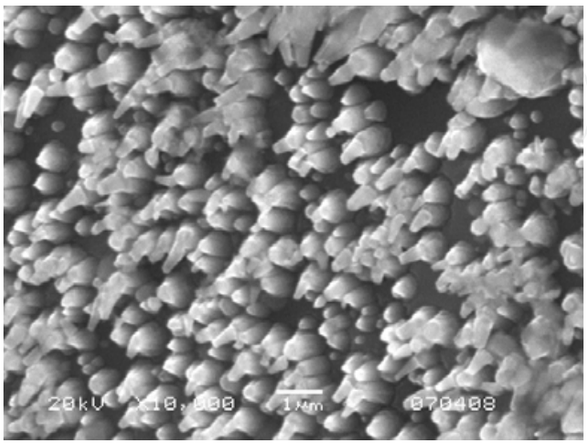

(c)

Fig. 15. Micrographs from: a) Ar/(N70-Ar30), b) Ar/(N50-Ar50), c) Ar/(N30-Ar70)

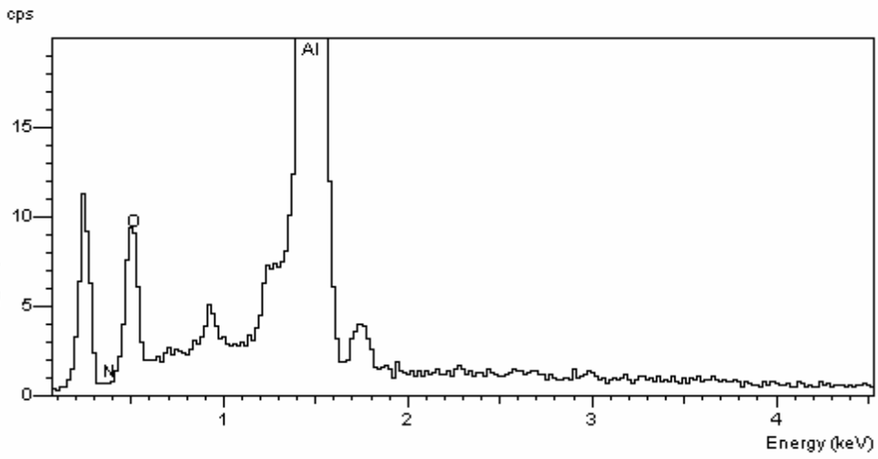

(a)

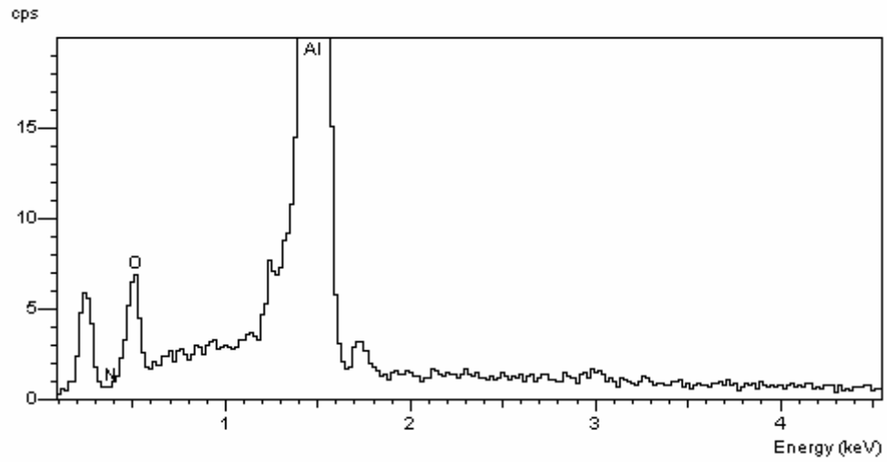

(b)

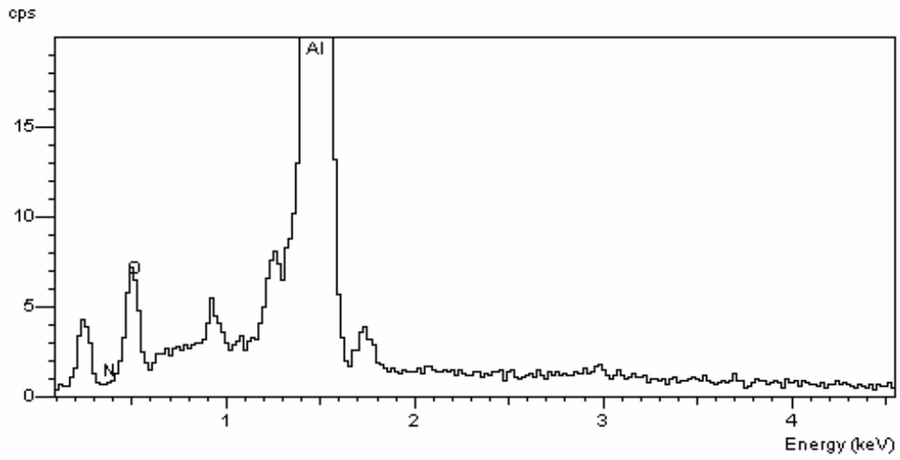

(c)

Fig. 16. Aluminium spectra from: a) Ar/(N70-Ar30), b) Ar/(N50-Ar50), c) Ar/(N30-Ar70)

Figure 17 shows that the greatest rugosity is achieved by the Ar/(N50-Ar50) sample which, at the same time, presents the lowest (290 nm) hardness (figure 18). The Ar/(N70-Ar30) sample reached an average value of 267 nm despite the maximal N concentration in the mixture and the consequent ion impact on the piece. The Ar/(N30-Ar70) sample obtained an R_a value of 195 nm: the lowest in the present experiment.

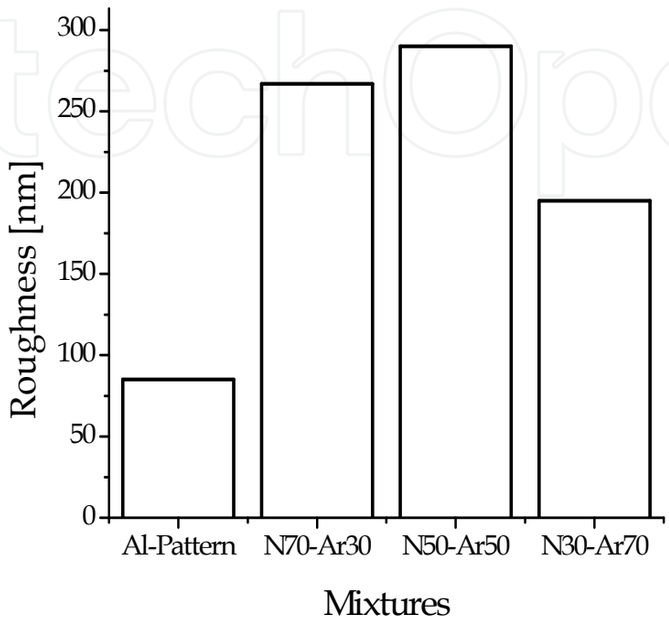

Fig. 17. Rugosity

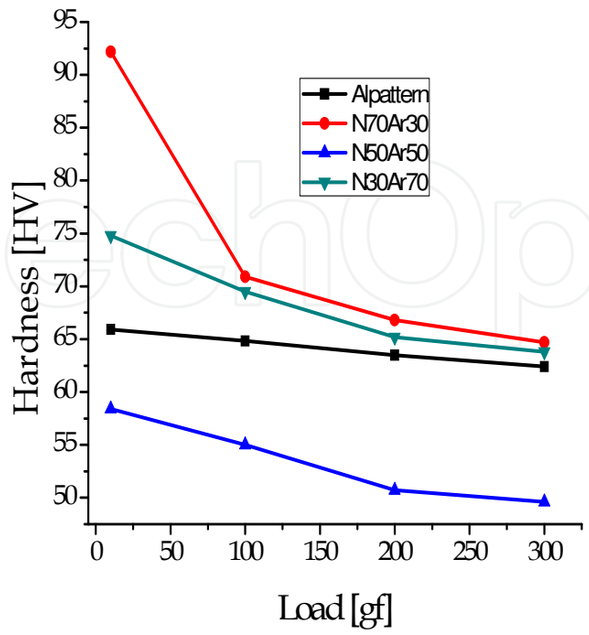

Fig. 18. Hardness

As follows from the hardness plot in figure 18, the maximal enhancement, up to 62HV0.1 at a 100 g load, was achieved with the highest nitrogen concentration mixture Ar/(N70-Ar30). By contrast, the Ar/(N30-Ar70) and Ar/(N50–Ar50) treated samples measured 60HV0.1 and 35HV0.1, respectively.

A comparative view of the diffractogrames shown in figure 19 indicates that the relative intensity of the Al peak at 2θ = 38.47° attained with the Ar/(N50-Ar50) mixture, decreases when the Ar/(N70-Ar30) and Ar/(N30-Ar70) ones are used (figures 19.a and 19.c). Quite the opposite with respect to the peak at 78.23° (figure 19.b) whose intensity is greater than those seen in figure 19.a y 19.c. The latter may be due to a low concentration of compounds like AlN and Al_2O_3 and to Al peaks either intrisically moderate or missing (such as the one expected at 2θ = 65.13°). Likewise, the Ar/(N50-Ar50) diffractogramme seen in figure 19.b, does not show the 2θ = 82.43° Al peak while the main Al peak is particularly reduced wich is ultimately attributable to the implantation process itself. The diffractogramme of figure 19.c points to the fact that a low N concentration favours the cubic phase of AlN at 2θ=41.80° (87-1053 JCPDS standard), 78.41° and 82.62° (46-1200 JCPDS standard).

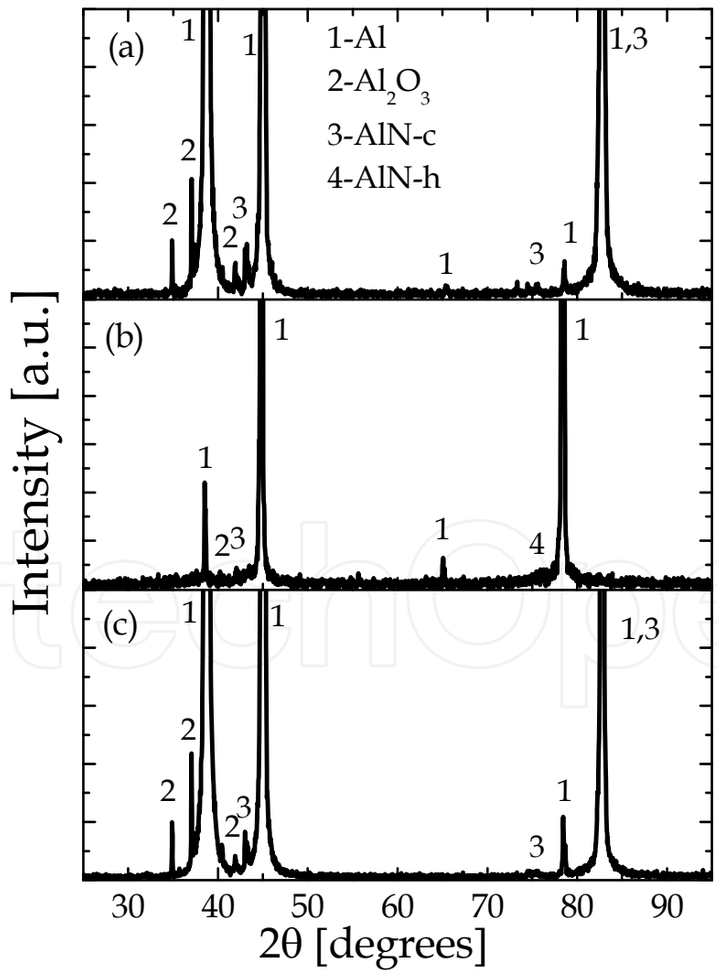

Fig. 19. Diffractogrammes a) Ar/(N70-Ar30), b)Ar/(N50-Ar50) c)Ar/(N30-Ar70)

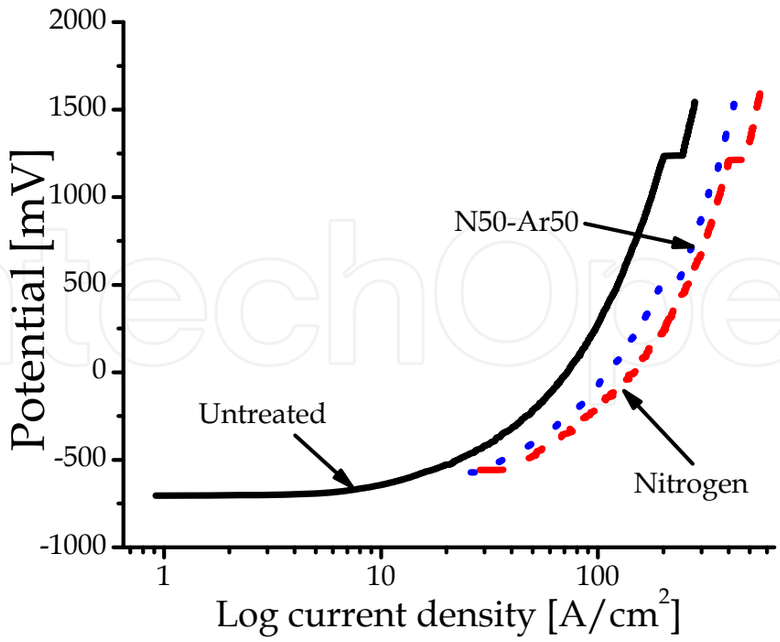

Fig. 20. Potentiodynamic polarization curves

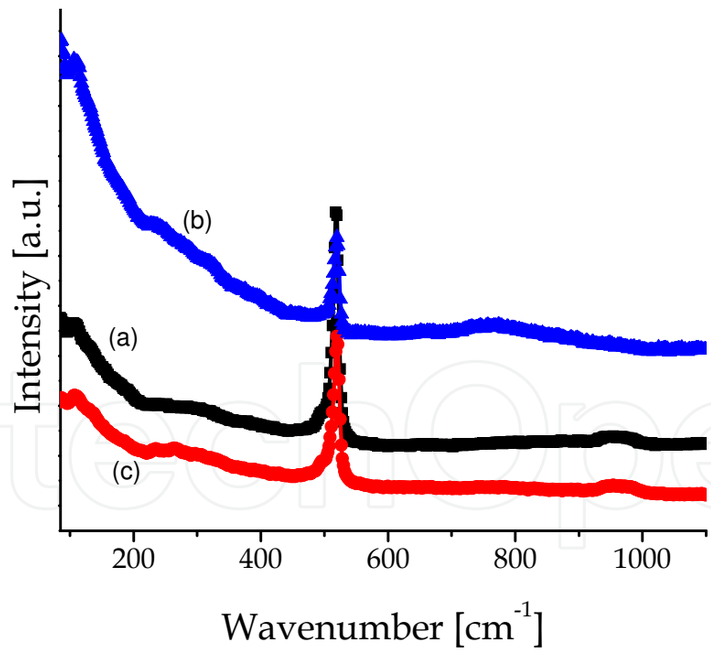

Fig. 21. Raman spectra (a) Nitrogen, (b) 50%N/50%Ar mixture and (c) 70%N/30%Ar

4.3 Corrosion analysis

Electrochemical potentiodynamic polarization tests were carried out within a cell containing 1 l of de-aerated 1.0N solution of H_2SO_4 as electrolyte. The measured results for untreated as well as treated samples are shown in figure 20. The more positive corrosion potential of the

treated samples indicates a more electrochemically noble surface and enhanced tolerance to corrosion. The treated sample response is quite similar, irrespective of the temperature and duration of the treatment.

4.4 Raman analysis

The samples treated with a mixture of nitrogen-argon were analyzed by means of Raman Spectroscopy in order to validate the results obtained from XRD (He-Ne laser at a 632.8 nm wavelength). Figure 21 shows the resulting Raman spectra for AlN. The 514 cm^{-1} peak, typical of AlN, is always visible, which coincides with the information provided by XRD diffractogrammes. Likewise, the spectra displayed in figure 4.a., where the absence of aluminium nitride is evident, are confirmed. The results of XRD and Raman spectroscopy show that the general sample improvement depends on the amount of N in the Ar/N mixture concentration.

5. Conclusions

The mechanical improvement of aluminium alloys by conventional nitriding techniques is considerably complex whereas plasma immersion ion implantation provides a simple and effective way to enhance the wear resistance and corrosion tolerance of these alloys. The present study has contributed to the knowledge of the AlN structure in 6061-T6 aluminia following a low energy (2-6 KeV) PIII at a 75-150 μs pulse width. Such a process approaches the conditions of a glow discharge where the anode is a 15 cm long stainless steel rod, 3.5 cm in diameter, placed horizontally at the top of the cylindrical 304 stainless steel vacuum chamber 60 cm high and 30 cm in diameter which, in turn, plays the role of cathode of the discharge. The latter is fed by a DC power supply with a maximum output power of 1200 W, specifically designed and constructed from a current-source converter operating in a resonant mode. Several previously optimized work gas compositions were used: pure nitrogen, 30% argon/70% nitrogen, 50% argon/50% nitrogen, 70% argon/30% nitrogen providing ion doses in the order of 10^{21} ions/cm^2. Samples were implanted at ~400°C for ~1 h periods. X-ray diffractometry, scanning electron microscopy, Vickers microhardness tests, profilometry, corrosion and Raman spectroscopy methods were applied to evaluate the treatment outcome. The highest microhardness values were achieved with the equal part gas mixture and a voltage bias. The greatest roughness was obtained by increasing the implantation pulse width up to 150 μs with the same mixture. The roughness seems to remain invariant when pure nitrogen is used provided that longer time implantation periods are completed. Increasing the surface microhardness of aluminium without jeopardizing its average rugosity depends critically on selecting the correct Ar and N proportions to be used in a very low voltage PIII.

An ostensible improvement on the AlN microhardness results from the presence of the hexagonal crystalline phase and the elimination of the cubic one, the characteristic peaks of AIN in the near surface having been confirmed by Raman spectroscopy. A compromise is to be established between rugosity and microhardness through the several variables in the process.

The optimal conditions characterised in the present study for the PIII treatment of 6061T6 aluminium samples can be summarised as plasmas made out of mixtures of argon with, at least, 50% nitrogen, applied once the sample temperatures reach around 450°C. Thus, the implantation of the aluminium samples results in the surface formation of nitrides. X ray

diffraction of the implanted pieces reveals the presence of AlN in the cp and hcp crystalline phases where the peak intensities increase along with the nitrogen content. The presence of the hexagonal phase has been detected when either pure nitrogen or a 50% mixture have been used, suggesting a correlation between the h phase and the enhanced microhardness. Raman spectroscopy has confirmed the signature peak of AlN and, in addition to XRD, shows that the general surface improvement is enhanced with the N proportion in the Ar/N mixture concentration.

A compromise between high hardness and low roughness in pure nitrogen is observed due to a competition between sputtering and nitriding after, at least, 1 hour of treatment. In particular, maximal microhardness values were found in samples treated with the equal part mixture. The best roughness was achieved with this gas mixture in all cases, although increasing along with the implantation pulse width up to a 300 nm peak at 150 μs. Such a performance can be maintained in a pure nitrogen plasma, provided that longer 1 hour implantation periods are performed.

6. Acknowledgment

The authors are grateful to the technical collaboration received from Israel Alejandro Rojas Olmedo, Hannalí Millán Flores, Everardo Efrén Granda Gutiérrez, María Teresa Torres Martínez, Pedro Angeles Espinoza and Isaías Contreras Villa,.

7. References

Anders André, editor. (2000), "Handbook of plasma inmersion implantation ion and deposition". Ed. John Wiley and Sons, ISBN 0-471-24698-0, USA

Conrad, J. R., (1987) Sheath thickness and potential profiles of ion-matrix sheaths for cylindrical and spherical electrodes, *Journal of Applied Physics*, Vol.: 62, No. 3, pp 777 – 779

Conrad J. R., Radtke J. L., Dodd R. A., Worzala Frank J. and Tran Ngoc C. (1987) Plasma source ion-implantation technique for surface modification of materials, *Journal of Applied Physics*, Vol 62, No. 11, pp. 4591-4596

Herman D. A., Gallimore A. D. (2008) An ion thruster internal discharge chamber electrostatic probe diagnostic technique using a high-speed probe positioning system, *Review Scientific Instruments*, Vol. 79, 013302, 10 pages.

Manova D., Mändl S. and Rauschenbach B. (2001), Oxygen behaviour during PIII-nitriding of aluminium, *Nuclear Instruments and Methods in Physics Research Section B: Beam Interactions with Materials and Atoms*, Vol. 178, No. 1-4, pp 291-296.

Selvaduray G., Sheet L. (1993) Aluminium nitride: review of synthesis methods Source, *Materials Science and Technology*, Vol. 9, No. 6, pp 463-473

Wang J. A., Bokhimi X., Morales A., Novaro O., López T. and Gómez R. (1999). Aluminum Local Environment and Defects in the Crystalline Structure of Sol-Gel Alumina Catalyst, *J. Phys. Chem. B,* Vol. 103, pp. 299-303

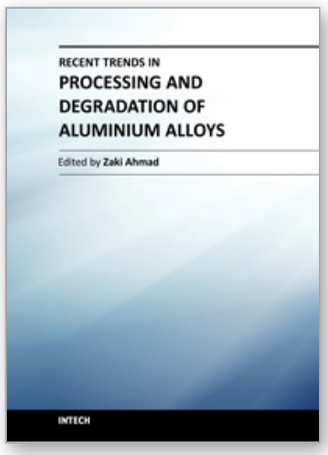

Recent Trends in Processing and Degradation of Aluminium Alloys
Edited by Prof. Zaki Ahmad

ISBN 978-953-307-734-5
Hard cover, 516 pages
Publisher InTech
Published online 21, November, 2011
Published in print edition November, 2011

In the recent decade a quantum leap has been made in production of aluminum alloys and new techniques of casting, forming, welding and surface modification have been evolved to improve the structural integrity of aluminum alloys. This book covers the essential need for the industrial and academic communities for update information. It would also be useful for entrepreneurs technocrats and all those interested in the production and the application of aluminum alloys and strategic structures. It would also help the instructors at senior and graduate level to support their text.

How to reference
In order to correctly reference this scholarly work, feel free to copy and paste the following:

Régulo López-Callejas, Raúl Valencia-Alvarado, Arturo Eduardo Muñoz-Castro, Rosendo Pena-Eguiluz, Antonio Mercado-Cabrera, Samuel R. Barocio, Benjamîn Gonzalo Rodrîguez-Méndez and Anibal de la Piedad-Beneitez (2011). PIII for Aluminium Surface Modification, Recent Trends in Processing and Degradation of Aluminium Alloys, Prof. Zaki Ahmad (Ed.), ISBN: 978-953-307-734-5, InTech, Available from: http://www.intechopen.com/books/recent-trends-in-processing-and-degradation-of-aluminium-alloys/piii-for-aluminium-surface-modification

INTECH
open science | open minds

InTech Europe
University Campus STeP Ri
Slavka Krautzeka 83/A
51000 Rijeka, Croatia
Phone: +385 (51) 770 447
Fax: +385 (51) 686 166
www.intechopen.com

InTech China
Unit 405, Office Block, Hotel Equatorial Shanghai
No.65, Yan An Road (West), Shanghai, 200040, China
中国上海市延安西路65号上海国际贵都大饭店办公楼405单元
Phone: +86-21-62489820
Fax: +86-21-62489821

IntechOpen